Creep and Relaxation Behavior of Woven Glass/Epoxy Substrates for Multilayer Circuit Board Applications

P. SHROTRIYA *and* N. R. SOTTOS

Department of Theoretical and Applied Mechanics
University of Illinois at Urbana-Champaign
Urbana, Illinois 61801

The creep behavior of a common woven glass/epoxy composite substrate for multilayer circuit board applications was characterized using dynamic mechanical analysis (DMA). The creep compliance was measured in both the warp and fill directions of the composite over a temperature range of 30°C to 155°C. The creep compliance of the neat FR-4 epoxy matrix was also characterized for comparison with the composite response. Master creep curves were obtained for the neat resin and the composite in the warp and fill directions assuming thermorheologically simple behavior and applying the time-temperature superposition principle. The creep data was fit to a Prony series and then converted to relaxation data in the Laplace domain. Micromechanical models were developed to predict the relaxation behavior of the woven glass/epoxy composite from the elastic properties and the geometry of the glass fabric and relaxation behavior of the neat resin. Model predictions were compared with experimental data.

1. INTRODUCTION

Dimensional stability of multilayer circuit boards has become an important issue in the electronic packaging industry. A typical multilayer construction, shown in *Fig. 1*, consists of several layers of woven glass-epoxy composite substrate, bonding sheets, and copper foil. Significant residual stresses develop during the manufacturing and post-manufacturing processes of the boards, which cause shrinkage and warpage. With increasing circuit densities, the amount of dimensional tolerance is significantly decreased and the number of circuit boards that pass quality standards also decreases. Dimensional changes in the boards also cause problems with solder connections and chip insertions, which significantly affect the reliability of the package.

The manufacture of multilayer circuit board consists of several stages. First, glass fiber bundles are woven into a fabric and impregnated with FR-4 epoxy resin to form a B-staged prepreg. Several different plain weave fabric styles are currently used in multilayer boards. The fabrics are often unbalanced, having different numbers of fiber bundles or different-size fiber diameters in the warp and fill directions. Because of the variation in fiber bundle sizes, the crimp of the fiber bundles is often unbalanced and depends on the fabric styles. Hence, different fabrics can have very different properties. A specified number (typically 1 or 2) of B-stage prepregs layers are then consolidated between two layers of copper in a hot press to form a C-staged core. The cores go through a series of etching and screening processes. Multilayer boards are then fabricated by relaminating alternating layers of C-staged cores, copper foil, and B-staged prepreg, which act as bonding sheets in a predetermined design. The inner layers of the board can shrink as much as 1000 ppm during relamination (1). Post-manufacturing processes such as solder masking, solder reflow, and wave soldering also generate residual stresses and strains.

The ability to accurately predict the residual stress state and to design more dimensionally stable circuit boards depends on accurate determination of the thermo-mechanical properties of the substrate. Several recent investigations have focused on experimental characterization and model prediction of substrate properties below the glass transition temperature of the resin. Sottos, Ockers, and Swindeman (2) investigated the influence of fabric geometry (bundle size, crimp, etc.) on the elastic moduli and coefficients of thermal expansion (CTE) of two common substrates for multilayer circuit boards. Wu, Guo, and Chen (3) and Yuan and Falanga (4) experimentally characterized the CTE of FR-4 laminates and employed a semi-empirical model to predict the data.

Presented at McNU'97 The Joint American Society of Mechanical Engineers (ASME), American Society of Civil Engineers (ASCE), Society of Engineering Science (SES) Summer Meeting.

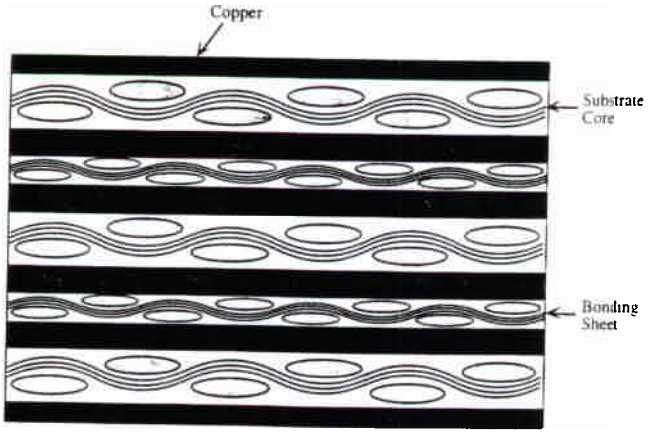

Fig. 1. Schematic of the multilayer circuit boards.

During relamination and subsequent soldering processes, the temperature of the woven glass/epoxy substrate exceeds the glass transition temperature of the epoxy matrix for extended periods of time. Extensive relaxation or creep can occur in the boards. In order to accurately predict the residual stresses and dimensional changes in the board, the time-temperature dependence of the substrate properties need to be well characterized. Wang, Daniel, and Gotro (5) generated master relaxation curves for one particular type of composite substrate and used the data in a viscoelastic analysis to predict warpage of the board. More recently, Chiang, McKenna, and Yuan (6) developed a simplified micromechanics model to examine the role of material viscoelasticity on the dimensional stability of a composite multilayer board. The board was modeled as two epoxy layers with a composite substrate inner layer in between. The outer layers were assumed to be isotropic, linear viscoelastic, while the inner layer were assumed to be an orthotropic, elastic composite. Given the large number of different combinations of substrate fabric styles used in the circuit board industry and the strong influence of the fabric weave, a more fundamental study of substrate creep and relaxation behavior is needed.

In this work, the creep compliance of a typical plain weave composite substrate along with the neat FR-4 resin are characterized using dynamic mechanical analysis (DMA). Master curves are obtained by horizontally shifting the measured creep compliance at various temperatures. Creep data are then converted to stress relaxation data in the Laplace domain. A general micromechanical model is developed to predict the relaxation behavior of the woven glass/epoxy composite from the elastic properties and the geometry of the glass fabric and relaxation modulus of the neat resin. Model predictions are compared with experimental data.

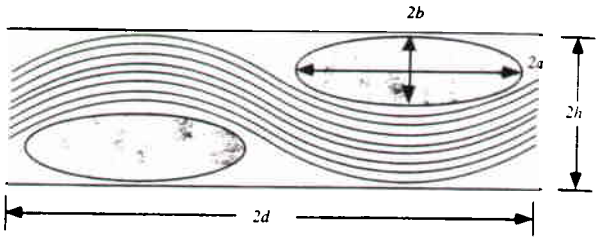

Fig. 2. Schematic of plain weave unit cell.

2. SUBSTRATE MATERIAL

The composite substrates used in circuit board applications consist of FR-4 epoxy matrix reinforced with a plain weave glass fabric. The plain weave is composed of two sets of orthogonal fiber bundles called the warp and fill. A schematic of the unit cell of the weave is shown in *Fig 2*. The viscoelastic response of the substrate is a function of the properties of the glass fiber bundles and the FR-4 matrix, as well as the geometry of the woven glass fiber bundles. In order to relate the geometry of the plain weave to the viscoelastic response, the microstructure of the fabric must first be characterized.

In this study, the properties of one common fabric style, 7628, were investigated. The 7628 style substrates were obtained in the form of commercially pressed boards from Polyclad Inc. The boards consisted of one layer of 7628 fabric sandwiched between two sheets of copper. Four 1" square sections were cut from the laminate and mounted so that either the fill or the warp direction was exposed. The samples were polished and carefully examined under an optical microscope for variations in the microstructure that might influence the viscoelastic properties of the substrate. Photomicrographs taken in the warp and fill directions are shown in *Fig. 3*.

Fig. 3a. Photomicrograph of 7628 laminate (70 ×) warp yarns parallel to the page, fill yarns perpendicular.

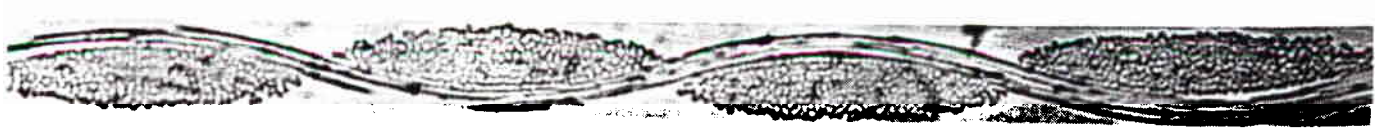

Fig. 3b. Photomicrograph of 7628 laminate (70 ×) fill yarns parallel to the page, warp yarns perpendicular.

Table 1. Measurements of Bundle Size and Crimp.

	Aspect Ratio a/b		Crimp h/d		Volume Fraction v_f	
	fill	warp	fill	warp	fill	warp
7628	7.26	5.26	0.083	0.053	0.194	0.268

The warp and fill bundles in *Figs. 3a* and *3b* have different sizes, crimp and volume fractions, which are described by a^k, b^k, d^k, and v^k (see *Fig. 2*) where $k = w$ or f for the warp and fill directions, respectively. The aspect ratio of the bundles $(a/b)^k$ and the crimp $(h/d)^k$ were carefully measured, and the results are listed in *Table 1*. Each value represents an average of ten different measurements. The aspect ratio and the crimp of the fill direction fiber bundles are larger than that of the warp direction bundles. No consistent variations in the bundle size or crimp were observed at varying locations across the board. Individual volume fractions of the warp and fill yarns are also listed in *Table 1*.

3. CHARACTERIZATION OF TIME TEMPERATURE BEHAVIOR

The time-temperature behavior of the neat FR-4 epoxy (no glass) and the composite substrate in both the warp and fill directions was characterized using a dynamic mechanical analyzer (Perkin-Elmer DMA 7e). The neat epoxy specimens were tested in three-point bending to determine the glass transition temperature, storage modulus, loss modulus, and creep compliance as a function of temperature. Because the substrates were only 0.17 mm thick, an extension fixture was used instead of the three point bend apparatus to characterize the creep compliance of the woven composite.

3.1 FR-4 Epoxy Matrix

Small rectangular beam specimens of FR-4 epoxy were prepared for testing on the Perkin-Elmer DMA 7e. *Figure 4* shows the three-point bending fixture along with the relevant dimensions of the test samples. Because of difficulties in obtaining the FR-4 epoxy directly, the specimens were prepared using the resin extracted from B-staged prepregs obtained from Polyclad. The prepregs were placed in a plastic bag and gently kneaded to remove the excess resin. A 10 cm by 10 cm square aluminum mold was filled with the extracted resin powder to a height of 1 cm. The mold was placed in a Tetrahedron MTP-14 hot press. for one hour at 160°C and a pressure of 0.1 MPa. The epoxy was pressed into a thin sheet of 2 mm thickness with low void content. Thin beams were cut from the epoxy sheet and then postcured at 150°C for 24 hours.

The storage and loss moduli of the postcured and non-postcured specimens was measured to demonstrate the effect of postcuring. The beam specimens were mechanically cycled at 1 Hz in three point bending as temperature was increased at the rate of 5°C/min from 20°C to 160°C. The storage and loss modulus are plotted in *Fig. 5* for postcured and non-postcured specimens. The temperature at which the loss modulus peaked was taken as the glass transition temperature (T_g). Postcuring of the matrix specimens shifted the T_g from approximately 129°C to 139°C. For comparison, the storage and loss modulus of the composite substrate in the fill direction were also measured for the same temperature range and plotted in *Fig. 6*. The T_g of the commercially pressed composite substrate was also close to 139°C. Hence, post-curing was necessary to raise the T_g of the neat epoxy samples.

The creep compliance of the epoxy specimens was then measured at several temperatures between room temperature (23°C) and the glass transition temperature (139°C). The beam specimens were loaded in three-point bending at a stress of 1 MPa for 20 minutes. The strain in the specimen was measured continuously to obtain the creep compliance of the specimen for the time period. Four different specimens were tested and the data averaged at each temperature. It was difficult to acquire creep data above the T_g using the three-point bend fixture owing to the high compliance of the epoxy at these temperatures.

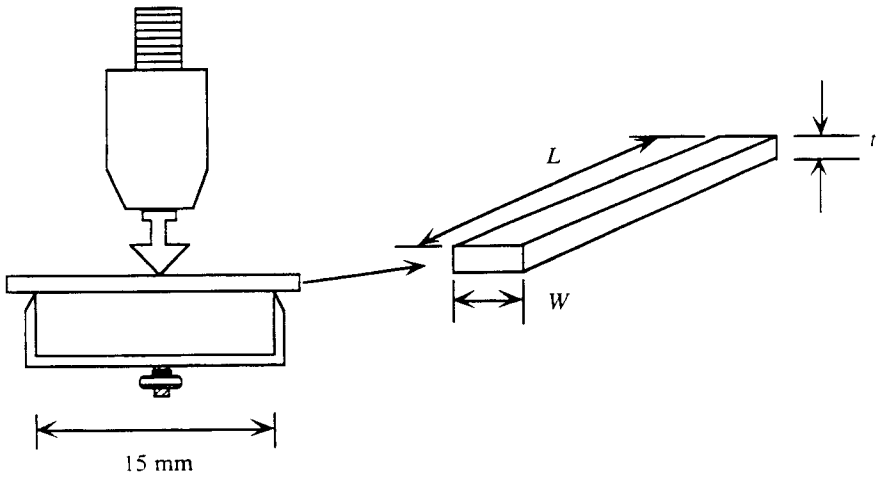

Fig. 4. FR-4 epoxy matrix specimen for three-point bending creep tests, t = 1.10 mm – 1.60 mm, L = 18.0 mm – 19.0 mm, W = 2.20 mm – 2.50 mm.

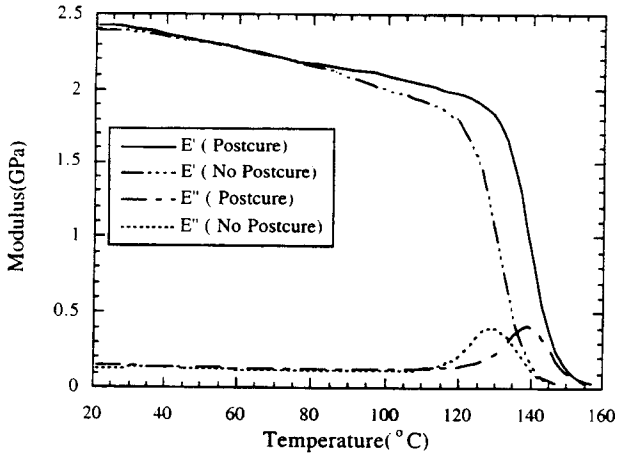

Fig. 5. Effect of postcure on FR-4 epoxy loss and storage moduli.

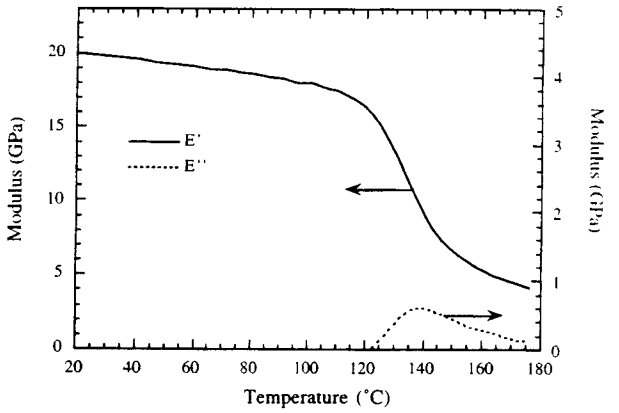

Fig. 6. Storage and loss modulus for the composite substrate in the fill direction.

The creep compliance of the epoxy at each temperature step is plotted versus the logarithmic time axis in *Fig. 7*. The data at each temperature in *Fig. 7* was then shifted to obtain a master creep compliance curve using the time-temperature superposition principle. The reference temperature was chosen as 30°C. The resulting master creep compliance curve is plotted as a function of the logarithmic reduced time in *Fig. 8*.

3.2 Composite Substrate

Uniaxial creep tests were performed to characterize the creep compliance of the woven composite using the Perkin-Elmer DMA 7e. Specimens were prepared from commercially pressed 7628 boards described in **Section 2**. The copper layers from the top and bottom of the laminate were removed using dilute nitric acid. Thin rectangular specimens were cut from the composite substrate such that the length was along either the fill or the warp direction. A schematic of the extension fixture along with the relevant dimensions of the sample is shown in *Fig. 9*.

The creep compliance of the composite substrate was measured in both the warp and fill directions at different temperatures between 30°C and 160°C. At each temperature, the specimens were loaded in tension to a stress of 10 MPa for 20 minutes. The strain in the sample was measured continuously to determine the creep compliance. Four different specimens were tested and averaged at each temperature. The individual creep curves for the composite are not presented, for the sake of brevity, but they have the same qualitative behavior as the matrix data in *Fig. 7*.

The creep compliance data for the different temperatures (not shown) were shifted using the time-temperature superposition principle to form the master creep compliance curves. The reference temperature was again chosen as 30°C. The master creep compliance curves of the composite substrate in the warp and fill directions are plotted in *Fig. 8* along with the master curve for the neat matrix.

The value of the unrelaxed compliance in the fill direction is significantly higher than in the warp direction. Also, the difference between the measured values

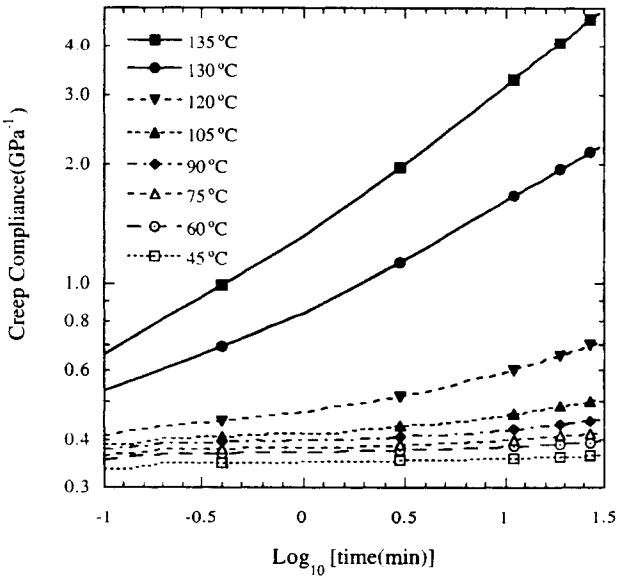

Fig. 7. Creep curves for the FR-4 matrix at different test temperatures.

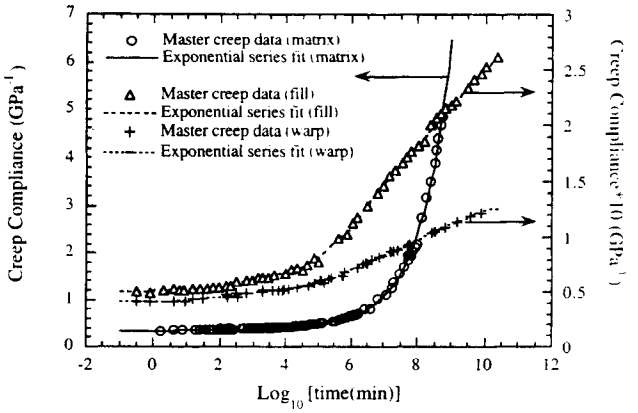

Fig. 8. Master creep curve for the FR-4 epoxy and the composite substrate in warp and fill directions. Reference temperature = 30°C.

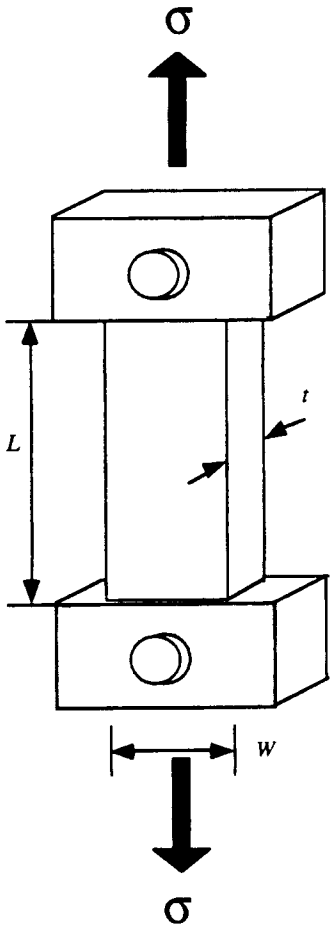

Fig. 9. Composite substrate specimen for uniaxial creep tests, t = 0.17 mm, L = 6.10 mm – 9.00 mm, W = 3.00 mm – 3.50 mm.

of the fully relaxed compliance and the unrelaxed compliance is higher in the fill direction than in the warp direction. This effect is due to the higher bundle crimp in the fill direction. Moreover, in both the fill and warp directions there is a large difference between the fully relaxed and unrelaxed compliance, indicating significant creep along both weave directions in the composite.

3.3 Shift Factors

The creep compliance master curves for the matrix and the composite substrate are formed by shifting the creep data according to the time temperature superposition principle. Examination of the raw creep data and various trials with the shifting showed that horizontal shifting alone was adequate to form the master curves. Following Wang *et al.* (5), it was assumed that both the epoxy and composite are thermorheologically simple. The curves are modeled using the reduced time ξ defined by

$$\xi = \int_0^t a_T(T)d\tau \tag{1}$$

where $a_T(T)$ is the temperature shift function. The logarithm of the shift function for the matrix and composite substrate in the warp and fill directions is plotted as a function of inverse temperature in *Fig. 10*. As expected, the shift functions for all three cases show similar behavior. The logarithm of the shift function is bilinearly dependent on the reciprocal of the temperature and is fit to the following equation,

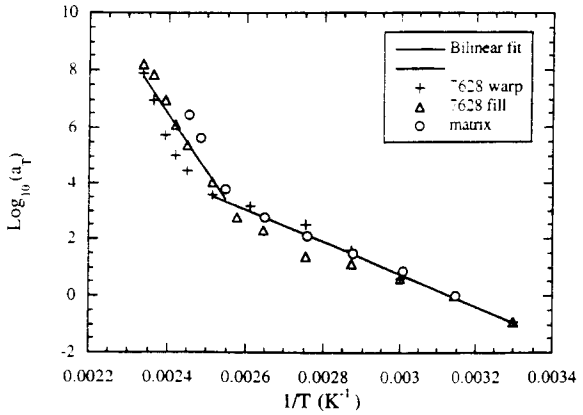

Fig. 10. Bilinear dependence of the shift factors on inverse temperature.

$$Log(a_T(T)) = \begin{cases} -\dfrac{5757}{T} + 18 & T < 393K \\ -\dfrac{20661}{T} + 56 & T > 393K \end{cases} \tag{2}$$

where T is the temperature in Kelvin.

4. STRESS RELAXATION MODULUS

The viscoelastic stress relaxation modulus was determined by converting the creep compliance data in the Laplace domain. In the Laplace domain, the creep compliance $J(s)$ and the stress relaxation modulus $E(s)$ are related by

$$J(s)E(s) = \frac{1}{s^2} \tag{3}$$

Once *Eq 3* is solved for $E(s)$, the stress relaxation modulus in the time domain can be obtained by the inverse Laplace transform,

$$E(t) = L^{-1}(E(s)) \tag{4}$$

The creep compliance curve for viscoelastic materials is usually modeled by a power law (7)

$$J(\xi) = J_0 + J_1[\xi]^q \tag{5a}$$

or by a stretched exponential function (also referred to as KWW function) (6)

$$J(\xi) = J_0 e^{\left[-\left(\frac{\xi}{\tau}\right)^q\right]} \tag{5b}$$

or by a series of discrete exponential terms (8–10) such as

$$J(\xi) = J_r - \sum_{i=1}^{n} J_i e^{\left[\frac{-\xi}{\tau_i}\right]} \tag{5c}$$

where J_0 is the unrelaxed compliance, J_1 is a compliance coefficient, J_r is the fully relaxed compliance, ξ is

the reduced time, q is a material constant, and τ_i are the discrete retardation times. The experimental data cannot be fit to *Eq 5a* over the whole temperature range using a single value of q. In addition, the inverse Laplace transform for the stress relaxation modulus calculated from *Eq 5a*, cannot be found analytically. For the stretched exponential function, the Laplace transform of the creep compliance can be found analytically only if q is equal to 0.5. For the exponential series model, an exact inverse Laplace transform for the stress relaxation modulus exists. The resulting stress relaxation modulus is another series of exponential terms that provides for computational convenience in viscoelastic solution techniques such as the recursive formulation for time superposition integral calculations (8–10).

As a result, the creep compliances of the matrix and the composite substrate in the fill and warp directions were modeled using *Eq 5c*. An exponential series of nine to twelve terms was fit to the creep data, and the discrete retardation times were found by nonlinear curve fitting using the simplex technique implemented in Matlab®. *Figure 8* shows the nonlinear curve fits of the matrix and composite substrate creep data. The discrete retardation times and corresponding compliance coefficients are listed in *Table 2* for the matrix and in *Tables 3* and *4* for the fill and the warp directions of the composite substrate.

The stress relaxation modulus for the matrix and the composite substrate were obtained in the time domain using *Eqs 3* and *4* and had the following form,

$$E(\xi) = E_r + \sum_{i=1}^{n} E_i e^{\left[\frac{-\xi}{\lambda_i}\right]} \qquad (6)$$

where E_r is the fully relaxed modulus and λ_i are the discrete relaxation times. The stress relaxation modulus of the matrix and the composite substrate in the fill and the warp directions is plotted in *Fig. 11*. The calculated λ_i values and corresponding coefficients for the matrix and the fill and warp direction of the composite substrate are listed in *Tables 5, 6,* and *7* respectively.

5. VISCOELASTIC MICROMODELING

A wide variety of fabric styles are used in woven composite substrates for multilayer circuit board applications. Because experimental characterization of all the different substrate types is prohibitive, micromechanical models for predicting the viscoelastic properties from fiber, resin, and weave properties would be extremely useful. While there are several models for predicting viscoelastic properties of composites, most were developed for unidirectional aligned fiber composites. These models utilize the analogy between the equations of elasticity and the Laplace transformed linear viscoelastic equations (12). Viscoelastic mixing rules are obtained in the Laplace domain by replacing the elastic components in a given elastic model by their Laplace transform counterparts. The time dependent properties of the composite are then approxi-

Table 2. Retardation Times and Compliance Coefficients for FR-4 Matrix.

i	J_i (GPa^{-1})	τ_i (min)
J_r	1.12e+01	
1	8.99e−03	5.64e−02
2	1.21e−02	1.04e+00
3	1.58e−02	1.71e+01
4	2.16e−02	2.62e+02
5	2.99e−02	3.31e+03
6	4.58e−02	3.21e+04
7	7.66e−02	2.53e+05
8	1.33e−01	1.52e+06
9	2.38e−01	7.46e+06
10	4.47e−01	3.22e+07
11	1.07e+00	1.45e+08
12	8.76e+00	1.62e+09

Table 3. Retardation Times and Compliance Coefficients for Composite Substrate in the Fill Direction.

i	J_i (GPa^{-1})	τ_i (min)
J_r	2.71e−01	
1	9.32e−04	1.53e+00
2	4.31e−03	7.68e+01
3	5.04e−03	4.62e+02
4	6.91e−03	6.62e+03
5	2.25e−02	1.06e+05
6	3.96e−02	1.88e+06
7	3.34e−02	1.55e+07
8	3.73e−02	1.88e+08
9	3.22e−02	1.73e+09
10	3.83e−02	1.61e+10

Table 4. Retardation Times and Compliance Coefficients for Composite Substrate in the Warp Direction.

i	J_i (GPa^{-1})	τ_i (min)
J_r	1.26e−01	
1	3.81e−03	1.61e+01
2	5.48e−03	5.55e+02
3	2.29e−03	9.09e+03
4	5.62e−03	6.25e+04
5	1.32e−02	6.89e+05
6	1.33e−02	6.06e+06
7	1.55e−02	1.00e+08
8	1.05e−02	5.49e+08
9	1.57e−02	5.00e+09

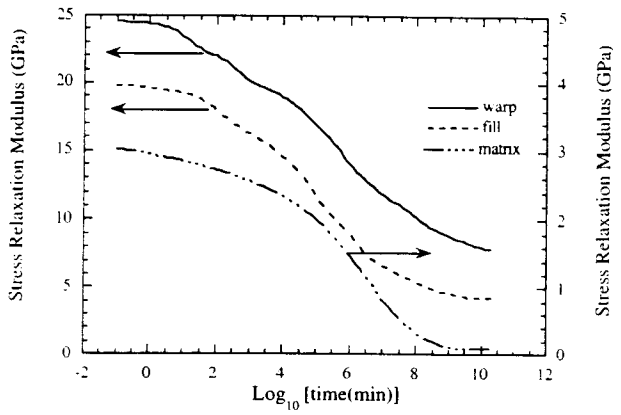

Fig. 11. Stress relaxation modulus of the matrix and the composite substrate in the warp and fill directions. Reference temperature = 30°C.

Table 5. Relaxation Times and Stress Relaxation Coefficients for FR-4 Matrix.

i	E_i (GPa)	λ_i (min)
E_r	8.90e−02	
1	8.40e−02	5.48e−02
2	1.06e−01	1.01e+00
3	1.29e−01	1.64e+01
4	1.59e−01	2.47e+02
5	1.95e−01	3.06e+03
6	2.55e−01	2.89e+04
7	3.45e−01	2.15e+05
8	4.34e−01	1.19e+06
9	4.59e−01	5.26e+06
10	3.79e−01	2.03e+07
11	2.68e−01	7.82e+07
12	1.99e−01	4.17e+08

Table 6. Relaxation Times and Stress Relaxation Coefficients for Composite Substrate in the Fill Direction.

i	E_i (GPa)	λ_i (min)
E_r	4.27e+00	
1	3.61e−01	1.50e+00
2	1.56e+00	7.09e+01
3	1.46e+00	4.24e+02
4	1.73e+00	5.95e+03
5	3.78e+00	8.00e+04
6	3.39e+00	1.31e+06
7	1.46e+00	1.24e+07
8	1.12e+00	1.53e+08
9	6.73e−01	1.50e+09

Table 7. Relaxation Times and Stress Relaxation Coefficients for Composite Substrate in the Warp Direction.

i	E_i (GPa)	λ_i (min)
E_r	7.91e+00	
1	2.11e+00	1.50e+01
2	2.47e+00	5.00e+02
3	9.00e−01	9.09e+03
4	1.89e+00	5.55e+04
5	3.26e+00	5.55e+05
6	2.13e+00	5.13e+06
7	1.85e+00	7.81e+07
8	9.10e−01	4.97e+08
9	1.05e+00	4.27e+09

mated by taking the inverse Laplace transform. Hence, the viscoelastic properties of the woven composites can be predicted by extending existing elastic micromechanical models into the Laplace domain. This approach was used by Govindarajan *et al.* (13) to predict the creep behavior of a graphite/epoxy woven composite.

A large number of micromechanical models for predicting the elastic properties of woven composites have been reported in the literature. The early models used classical lamination theory (CLT) to determine the properties of an idealized unit cell that represented the warp and fill geometry. Ishikawa and Chou (14–17) formulated two one-dimensional models for predicting the woven elastic properties of a woven ply. The first model, the mosaic model, views the fabric as an assemblage of two-ply cross-ply laminates, ignoring the continuity and undulation of the fiber bundles. The properties are integrated along the length of the unit cell. Averaging the compliances (iso-stress) yields the lower bound, while averaging the stiffnesses (iso-strain) yields an upper bound. The second model, the crimp model, uses CLT to determine the properties of a thin slice in the unit cell and integrates the properties along the length of the unit cell. A later model introduced in the work by Naik and Shembekar (18–20) and Shembekar and Naik (21, 22) is based on the crimp model. This model allows for gaps between the fiber bundles, in-plane misalignments between the piles, and the two-dimensional nature in a plain weave laminae.

Sottos, Ockers, and Swindeman (2) introduced two models to predict the properties of the woven laminates. The first model (EQLAM) is based on an equivalent laminate concept, which idealizes the woven fabric laminate as a symmetric three-ply cross-ply laminate. The properties of the outer plies are first calculated by combining warp fiber and resin properties via self-consistent micromechanics. Average ply properties are obtained by integrating over the length of the unit cell for the undulating warp fibers. Averaging the compliances (iso-stress) yields the lower bound, while averaging the stiffnesses (iso-strain) yields an upper bound. The inner-ply properties are calculated in a similar fashion by averaging the properties of the fibers in the fill direction. The overall properties of the laminate are then obtained using classical lamination theory. The second model (BLEND) does not use lamination theory to determine the final properties of the woven laminae. The fill fiber properties are first combined with resin properties via self-consistent micromechanics. The average fill ply properties then are determined by integration over the unit cell, as described above. The warp bundles are assumed to be reinforcing this intermediate fill ply. Average composite properties are then achieved by combining the warp fiber properties with the calculated properties for the intermediate fill ply using the Halpin-Tsai equations and integrating over the unit cell for the undulating warp fibers.

Lee and Harris (23) developed a mathematical model based on Euler-Bernoulli beam theory to predict the effective elastic properties of a composite with wavy layers. In this model, the wavy layers are modeled as curved beams and matrix layers are assumed to be elastic foundations. Under the application of a tensile force, the curved beam extends as a result of elastic deformation as well as the rigid body rotations associated with reduction of crimp. The elastic deformation is governed by the elastic properties of the beam while the rigid body motion is determined by the matrix surrounding the beam. The deformation of the curved beam is calculated by minimizing the total potential energy of the curved beam and the elastic foundation. The effective modulus of the composite is determined on the basis of the calculated displacement field.

In this study, two micromechanical models based on previously verified elastic models are utilized to pre-

dict the viscoelastic properties of the woven composites. Using these models, the stress relaxation response of the composite is calculated from the elastic modulus of the glass fibers, the geometry of the weave, and stress relaxation modulus of the matrix. Both models are summarized below.

5.1 Viscoelastic Equivalent Laminate Model

The first model is based on the equivalent laminate model (EQLAM) developed by Sottos, Ockers, and Swindeman (2). Shown schematically in *Fig. 12*, this model idealizes the woven fabric laminate as a symmetric three-ply cross-ply laminate. Following the elastic development of the model (2), the warp and the fill fibers are separated and represented as three different plies. The plies are arranged as a symmetric cross-ply laminate with a fill ply in the center of thickness b^f sandwiched between two warp plies of thickness $\frac{1}{2} b^w$ each, such that the total thickness, $t = b^w + b^f$. The effective stiffness matrix for each ply is calculated in the Laplace domain. First, the micromechanical relationships developed using the self-consistent field model (12) (see **Appendix**) are utilized to calculate the transversely isotropic properties of the plies, assuming that the fibers are straight. All the calculations are done in the Laplace domain using the Laplace transformed properties of the epoxy matrix and the glass fibers,

$$C_{ij}^{'k}(s) = f(sE_m(s), E_f) \tag{7}$$

where $k = w$ or f for warp and fill plies, $sE_m(s)$ is the Laplace transformed matrix modulus, and E_f is the fiber modulus. Using the weave geometry in *Table 1* to describe the undulation of the ply, coordinate transformations are used to find the properties $C_{ij}^{'k}(s,x)$ of a small portion dx at a position x. The transversely isotropic properties are integrated along the length of

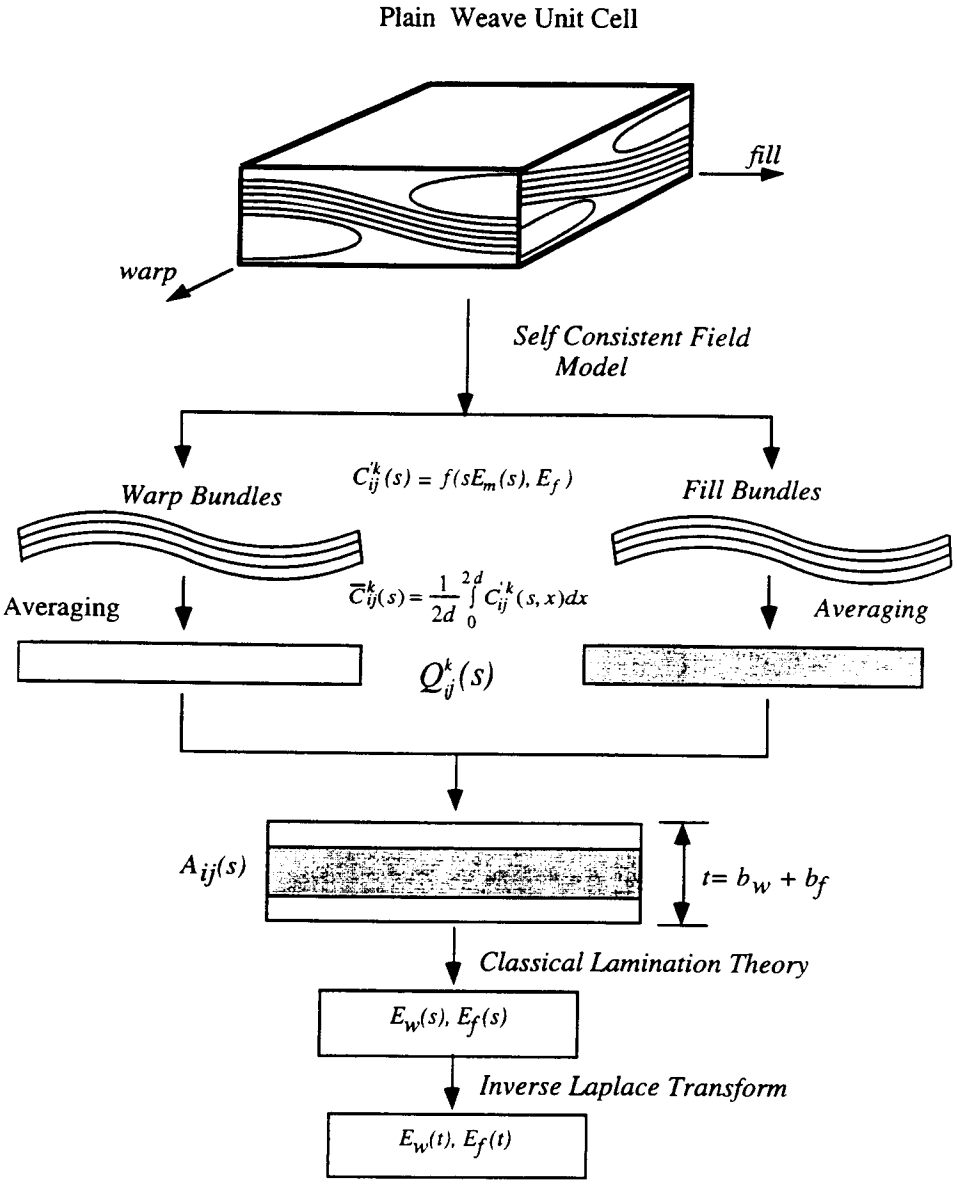

Fig. 12. Schematic of the equivalent laminate model (2).

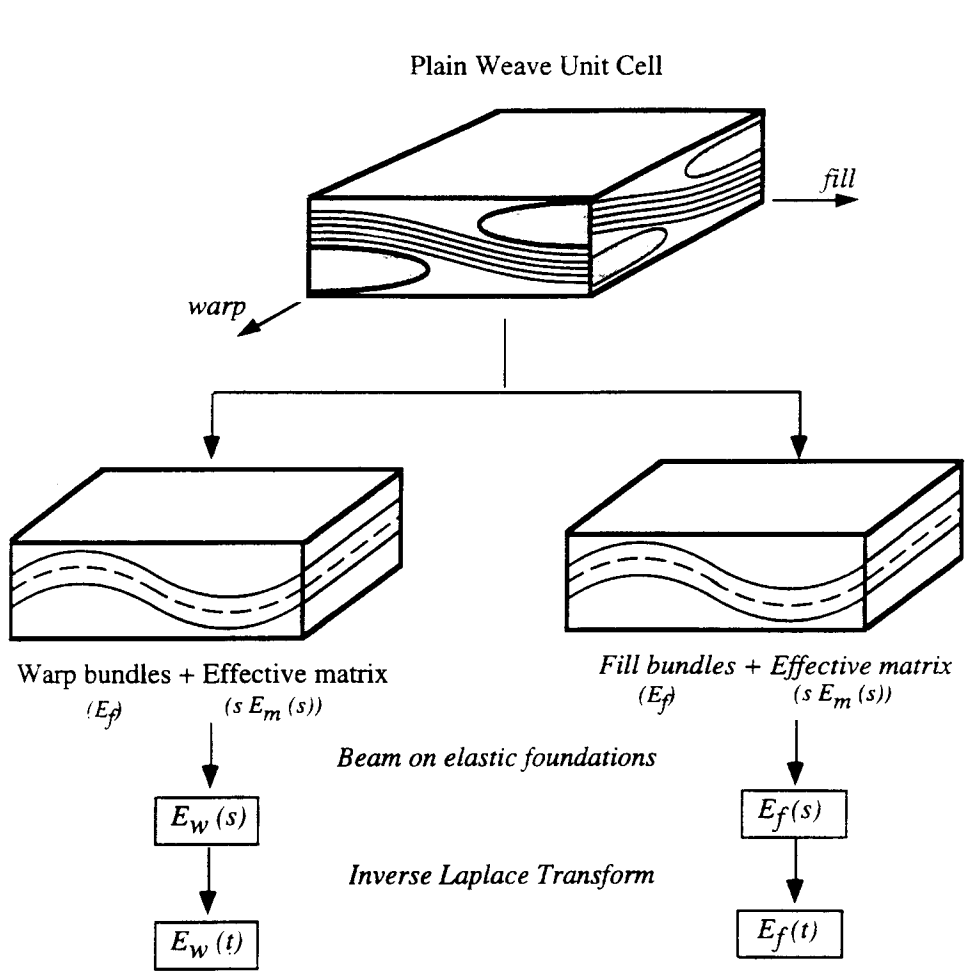

Fig. 13. Schematic of the curved beam model (23).

the representative volume element to yield the effective orthotropic properties of the plies,

$$\bar{C}_{ij}^{k}(s) = \frac{1}{2d}\int_{0}^{2d} C_{ij}^{'k}(s,x)dx \qquad (8)$$

The stiffness matrix A_{ij} of the laminate is formed using the classical lamination theory from the stiffness matrices of the plies. The Laplace transformed stress relaxation modulus of the laminate is obtained from the stiffness matrix. An inverse Laplace transform is performed to obtain the time dependent stress relaxation modulus of the woven composite.

5.2 Curved Beam on a Viscoelastic Foundation

The second model is based on the curved beam model presented by Lee and Harris (23). The model, shown schematically in *Fig. 13*, is a one-dimensional model to predict the stress relaxation modulus of the woven glass/epoxy composite. In the model, the woven glass fabric is separated into longitudinal and transverse fibers. The longitudinal fibers are modeled as a wavy layer, shown schematically in *Fig. 14*. The transverse fibers and the matrix are modeled as a homogenized matrix layer. The effective properties of the homogenized matrix layer, are calculated using the

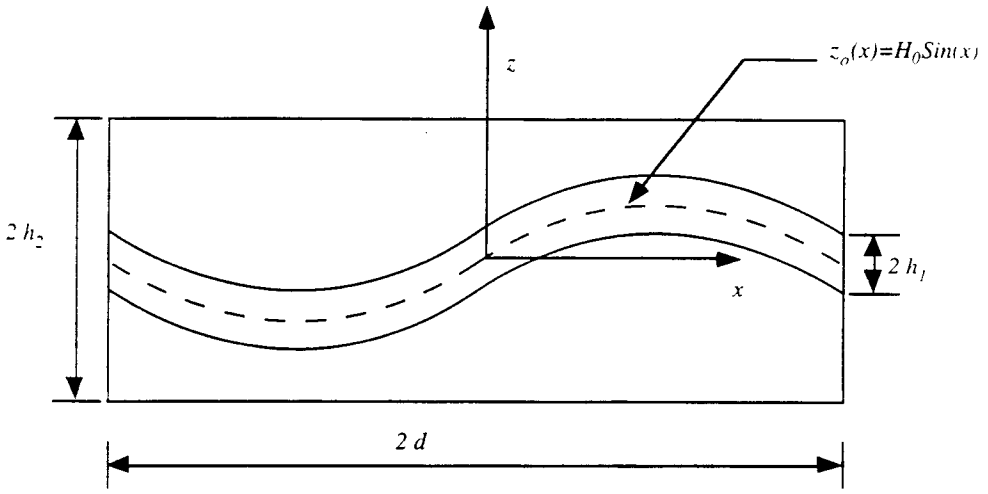

Fig. 14. Unit cell for the curved beam model.

self-consistent micromechanical relationships. Following the Lee and Harris model (23), the deformation of the undulating wavy layer embedded in the homogenized matrix is determined by minimizing the total potential energy in the Laplace domain. Schapery (24) and Jarzebski (25) recognized that a transform minimum principle could be established for a linearly viscoelastic material. The minimum in the Laplace domain can be inverted to time domain provided that the function is monotonic and there are no time dependent boundary conditions. This minimum provides reasonable bounds on the time dependent properties of the heterogeneous viscoelastic material (12).

Under the application of a tensile force P, the deformation $z_1(x)$ of the wavy layer from the centerline given by $z_0(x)$, is governed by the following differential equation,

$$E_f I \frac{d^4 z_1}{dX^4} - (\alpha^2 K_T + P) \frac{d^2 z_1}{dX^2} + K_L z_1 = P \frac{d^2 z_0}{dX^2} \quad (9)$$

where

$$K_T = 2(h_2 - h_1) G_m$$

$$K_L = \frac{2E_m}{(h_2 - h_1)}$$

$$\alpha = \frac{2h_1}{(h_2 - h_1)}$$

$$h_1 = V_f h_2$$

$$I = \frac{2}{3} h_1^3$$

and $E_f I$ is the flexural rigidity of the wavy layer, K_T is the torsional spring constant of the homogenized matrix layer, K_L is the linear spring constant of the homogenized matrix layer, α is a constant calculated from matrix deformation kinematics, G_m is the shear modulus of the homogenized matrix, E_m is the Young's modulus of the homogenized matrix, P is the tensile force per unit thickness, V_m and V_f are the volume fractions of the homogenized matrix and longitudinal fibers respectively, and H_0, h_0, h_1, and d are shown in *Fig. 14*. The solution of *Eq 9* is given by

$$z_1(x) = \frac{H_0 \sin(\pi x/d)}{1 + \gamma} \quad (10)$$

where

$$\gamma = \frac{\alpha^2 K_T}{P} + \left(\frac{\pi}{d}\right)^2 \frac{E_f I}{P} + \left(\frac{d}{\pi}\right)^2 \frac{K_L}{P}$$

Using *Eq 10* and assuming that $1/\gamma << 1$, the extension due to change of crimp, Δ_1, the extension due to elastic deformation of the wavy layer, Δ_2, and the total extension of the composite, Δ, are calculated as

$$\Delta_1 = \frac{\pi^2 H_0^2}{2d\gamma} \quad (11)$$

$$\Delta_2 = \frac{Pd}{2E_f h_1} \quad (12)$$

$$\Delta = \frac{\pi^2 H_0^2}{2d\gamma} + \frac{Pd}{2E_f h_1} \quad (13)$$

Therefore, the total strain in the matrix layer and the unit cell is (Δ/d) and in the wavy layer is (Δ_2/d). The total force per unit length on the unit cell is $(P + 2E_m \Delta/d(h_2 - h_1))$ and the apparent strain in the unit cell is (Δ/d). The modulus E_k (where $k = w$ or f) of the composite in the longitudinal direction is then calculated as

$$E_k = \frac{1}{\left(\left(\frac{\pi H_0}{d}\right)^2 \frac{1}{\mu} + \frac{1}{E_f V_f}\right)} + E_m V_m \quad (14)$$

where

$$\mu = \left(\frac{V_f^2}{1 - V_f}\right) 2G_m + \left(\frac{\pi h_2}{2d}\right) \frac{2}{3} E_f V_f^3 + \left(\frac{2d}{\pi h_2}\right) \frac{2E_m}{1 - V_f} \quad (15)$$

The Laplace transformed stress relaxation modulus of the woven composite is calculated by replacing the homogenized matrix properties E_m and G_m by the corresponding Laplace transformed viscoelastic properties $sE_m(s)$ and $sG_m(s)$ in *Eq 14*. Finally, the time dependent stress relaxation modulus is obtained by inverse Laplace transform.

6. COMPARISON OF MODEL PREDICTIONS AND EXPERIMENT

The experimental unrelaxed moduli in the warp and fill directions of the 7628 composite are first compared with values predicted by elastic micromodels reported in the literature. Calculations are made with the equivalent laminate model (EQLAM) developed by Sottos, Ockers, and Swindeman (2) and the curved beam model (BEAM) developed by Lee and Harris (23), using the elastic properties of the glass fibers and FR-4 epoxy matrix listed in *Table 8* and the measurements of bundle crimp, size, and volume fraction in *Table 1*. Upper and lower bounds on the unrelaxed modulus are predicted by the EQLAM model assuming iso-strain and iso-stress conditions, respectively. Model results are compared with the experimental values in *Table 9*.

The EQLAM model predictions effectively bound the unrelaxed modulus values within experimental error. The curved beam model proposed by Lee and Harris (23) predicts values slightly lower than the experimen-

Table 8. Elastic Properties of the Glass Fibers and Unrelaxed Properties of FR-4 Epoxy.

	Glass Fiber	FR-4 Epoxy
E (GPa)	72.3	3.05
ν	0.22	0.33

Table 9. Unrelaxed Modulus of 7628 Composite Substrate.

	E_k (GPa)	
	Warp	Fill
Experiment	24.5 ± 0.5	19.8 ± 0.5
EQLAM (UP)	25.1	20.9
EQLAM (LO)	23.4	18.2
BEAM	23.6	19.4

tal data. This model is one-dimensional and does not account for the two-dimensional interlacing of the warp and the fill fibers, which may underpredict the modulus values.

The full stress relaxation response of the 7628 composite substrate is predicted with the viscoelastic models developed in **Section 5**. The matrix stress relaxation modulus plotted in *Fig. 11* (values given in *Table 5*), and the geometric properties from *Table 1* are substituted into the viscoelastic equivalent laminate (VQLAM) and the curved beam (VBEAM) models to calculate the composite stress relaxation moduli. The predicted response is compared with the experimental data in *Figs. 15* and *16* for the fill and warp directions, respectively. Because of slight differences in the prediction of the unrelaxed response discussed above, the curves in *Figs. 15* and *16* are normalized by the corresponding value of the unrelaxed modulus. Both the equivalent laminate model and the curved beam model significantly under predict the relaxation of the woven composite.

Experimental error may account for some of the discrepancy between the experimental data and the model predictions. The inability to measure the creep response of the matrix at temperatures above T_g may introduce experimental error in the matrix shift factors near the T_g. Comparisons of the matrix data with composite data successfully measured at temperatures above T_g indicate the experimental error could be as large as two decades in the data (see *Fig. 10*). Even though the shift factor error is potentially significant, it cannot account for the large difference between the model predictions and experimental data.

The equivalent laminate model assumes that the geometry of the woven glass fabric does not change during deformation of the composite. The predicted decrease in the composite relaxation moduli is due solely to the matrix relaxation. Any additional relaxation due to changes in the fiber crimp is neglected. As a result, the model predicts almost no decrease in moduli with time. The curved beam model does account for the deformation of the composite resulting from extension of the curved beam as well as rigid body motion associated with the change of fiber crimp. A more pronounced decrease in moduli is predicted but not nearly as large as observed experimentally.

The comparison of the predicted response with experimental data indicates the relaxation behavior of the woven fabric is much more complex than the model representations. In particular, the experimental measurement of fully relaxed modulus is surprisingly lower than the values predicted by the models. For the fully relaxed case, the model predictions are essentially the response of the woven glass fabric without any matrix contribution. This difference suggests that the fabric deformation may be governed by mechanisms not accounted for in taking the Laplace transform of elastic micromodels. Further investigations of the unit cell deformation are necessary to fully understand the mechanisms governing the relaxation behavior of the woven composite.

7. CONCLUSIONS

The creep compliance of the 7628 style woven glass/epoxy composite was measured in both fill and warp directions over a temperature range of 30°C to 155°C. The creep compliance of the composite was significantly higher in the fill direction because of higher bundle crimp. Master creep curves were obtained for the composite in the warp and fill directions as well as the neat resin, assuming thermorheologically simple behavior and applying the time-temperature superposition principle. The shift factors for all the three cases showed similar behavior. The logarithm of the shift factor was found to be bilinearly dependent on

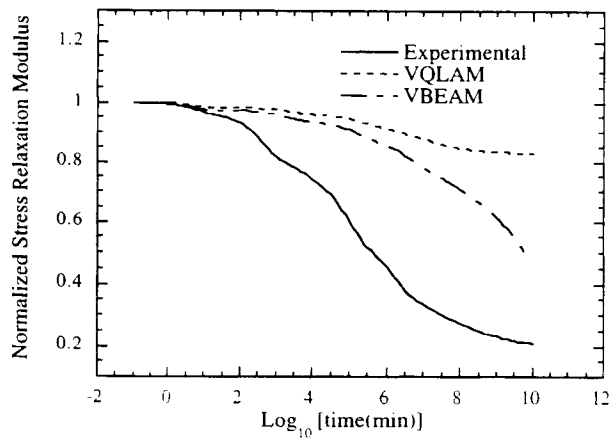

Fig. 15. Comparison of the experimental and predicted composite stress relaxation modulus in the fill direction.

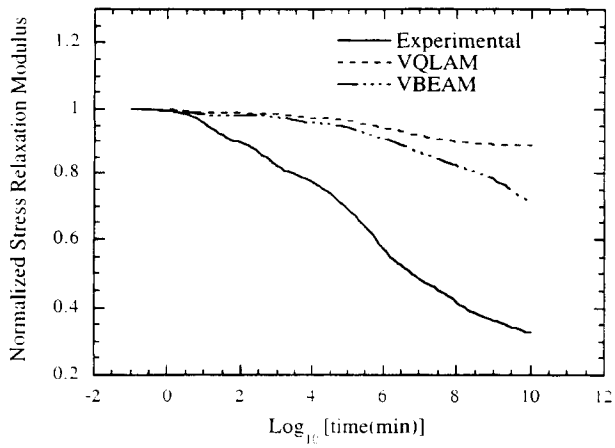

Fig. 16. Comparison of the experimental and predicted composite stress relaxation modulus in the warp direction.

the reciprocal of the temperature. The creep data was fit to a prony series and then converted to relaxation data in the Laplace domain.

Two micromechanical models were developed to predict the relaxation behavior of the woven glass/epoxy composite from the geometry of the glass fabric and properties of glass fibers and resin. The geometry of the 7628 style weave was carefully characterized. The measured geometric properties of the woven fabric and the matrix relaxation modulus were substituted into models to predict the relaxation behavior of 7628 style woven glass/epoxy composite. The micromechanical models predicted the unrelaxed modulus close to the experimental results but greatly underpredicted the relaxation of the composite. Comparison of the model predictions with the experimental data clearly indicates that the relaxation modulus of the composite is dependent not only on the relaxation of the matrix but also on geometric changes in the woven fabric bundles. Two-dimensional models that can accurately incorporate the influence of changes in fiber crimp are necessary for improved predictions of the composite relaxation moduli.

APPENDIX

Both models presented in this paper utilize the self-consistent field model to calculate effective properties of the unidirectional fiber composites. Details of the modulus are discussed by McCullough and Whitney (12). The relevant equations used to predict the effective composite properties in the current work are summarized below.

1. Longitudinal Young's Modulus (E_1):

$$E_1 = E_f v_f + E_m v_m \tag{16}$$

2. Poisson's Ratio (υ_{12})

$$\upsilon_{12} = \upsilon_f v_f + \upsilon_m v_m \tag{17}$$

3. In-plane Shear Modulus (G_{12})

$$G_{12} = G_m \frac{[(G_f + G_m) + (G_f - G_m)v_f]}{[(G_f + G_m) - (G_f - G_m)v_f]} \tag{18}$$

4. Transverse Shear Modulus (G_{23})

$$G_{23} = \frac{G_m[k_m(G_m + G_f) + 2G_f G_m - k_m(G_f - G_m)v_f]}{[k_m(G_m + G_f) + 2G_f G_m - (k_m - 2G_m)(G_f - G_m)v_f]} \tag{19}$$

5. Plane Strain Bulk Modulus (k_{23})

$$k_{23} = \frac{(k_f + G_m)k_m - (k_f - k_m)G_m v_f}{(k_f + G_m) - (k_f - k_m)v_f} \tag{20}$$

6. Transverse Young's Modulus (E_2)

$$E_2 = \frac{1}{\frac{1}{4k} + \frac{1}{4G_{23}} + \frac{\upsilon_{12}^2}{E_1}} \tag{21}$$

In the relations above, E_p, G_p, k_p, υ_p, and v_p are Young's modulus, shear modulus, bulk modulus, Poisson's ratio, and volume fraction, respectively, and $p = m$ or f for matrix and fiber.

ACKNOWLEDGMENTS

The authors gratefully acknowledge the financial support of Owens Corning Fiberglas, technical assistance from Doug Lyle at Owens Corning and the donation of material by Polyclad Inc.

REFERENCES

1. R. Holmes, *IPC Printed Circuit Expo 1996*. Northbrook, Illinois (1996).
2. N. R. Sottos, J. M. Ockers, and M. Swindeman, *J. Electronic Packaging*, in press (1998).
3. T. Y. Wu, Y. Guo, and W. T. Chen, *IBM J. Res. Develop.*, **37**, 621 (1993).
4. J. Yuan and L. A. Falanga, *J. Reinf. Plast. Compos.*, **12**, 489 (1993).
5. T. M. Wang, I. M. Daniel, and J. T. Gotro, *J. Compos. Mater.*, **26**, 883 (1992).
6. M. Y. M. Chiang, G. B. McKenna, and J. Yuan, *Polym. Eng. Sci.*, **34**, 1815 (1994).
7. Y. Weitsman, *J. Appl. Mech.*, **46**, 583 (1979)
8. S. Roy and J. N. Reddy, *Computers & Structures*, **29**, 1011 (1988)
9. Y. K. Kim and S. R. White, *Polym. Eng. Sci.*, **36**, 2852 (1996).
10. R. L. Taylor, K. S. Pister, and G. L. Goudreau, *Int. J. Num. Meth. Eng.*, **2**, 45 (1970).
11. S. R. White and Y. K. Kim, *J. Compos. Mater.*, in press (1997).
12. J. M. Whitney and R. L. McCullough, *Micromechanical Material Modeling, Delaware Composites Design Encyclopedia, Vol. 2*, Technomic Publishing Co., Lancaster, Pennsylvania (1990).
13. S. Govindrajan, N. A. Langrana, and G. J. Weng, *Polym. Compos.*, **17**, 353 (1996).
14. T. Ishikawa and T.-W. Chou, *J. Compos. Mater.*, **16**, 2 (1982).
15. T. Ishikawa and T.-W. Chou, *J. Mater. Sci.*, **17**, 3211 (1982).
16. T. Ishikawa and T.-W. Chou, *AIAA J.*, **21**, 1714 (1983).
17. T. Ishikawa and T.-W. Chou, *J. Compos. Mater.*, **17**, 92 (1983).
18. N. K. Naik and P. S. Shembekar, *J. Compos. Mater.*, **26**, 2196 (1992).
19. N. K. Naik and P. S. Shembekar, *J. Compos. Mater.*, **26**, 2522 (1992).
20. N. K. Naik and P. S. Shembekar, *J. Compos. Tech. Res.*, **15**, 34 (1993).
21. P. S. Shembekar and N. K. Naik, *J. Compos. Mater.*, **26**, 2226 (1992).
22. P. S. Shembekar and N. K. Naik, *J. Compos. Tech. Res.*, **15**, 23 (1993).
23. J. W. Lee and C. E. Harris, *J. Compos. Mater.*, **22**, 717 (1988).
24. R. A. Schapery, "Viscoelastic Behavior and Analysis of Composite Materials," in *Composite Materials, Vol. 2*, Academic Press, New York (1974).
25. G. J. Jarzebski, PhD dissertation, University of Delaware, Department of Chemical Engineering (1982).